

Numerical Study of a 3D Kinetic Detachment Flow in the Near-Wake of an Ahmed Body

Tientcheu-Nsiewe Max-well¹, Tcheukam-Toko Denis², Murzyn Frédéric³

¹UFD-PAI, ENSAI, University of Ngaoundéré, Cameroon

²CoITech, University of Buea, Cameroon

³CERIE –ESTACA parc universitaire Laval-Changé, France

(¹maxwelltientcheunsiewe@gmail.com, ²tcheukam_toko@yahoo.fr, ³Frederic.MURZYN@estaca.fr)

Abstract- Reducing the impact of cars on air pollution is now a major concern for car manufacturers. Several solutions are envisaged. Among which is the reduction of the drag. This reduction goes through a characterization of the flow of air around the vehicle during its displacement. Since the work of Ahmed S. et al., In 1984, many studies have emerged. This has made it possible to change vehicle configurations and considerably reduce their consumption. Nowadays, we are no longer satisfied with only proposing aerodynamic vehicle shapes, we are interested in controlling the flow around the vehicle in order to combine comfort and optimization of fuel consumption. The next work focuses on the active part of the control. It consists of a 3D numerical study of the coupling control of the underfloor flow and continuous blowing control downstream of Ahmed's body. The drag reductions obtained are more than satisfactory.

Keywords- Numerical Study, Kinetic Detachment, Near Wake, Ahmed Body

I. INTRODUCTION

In the last century, the development of the chemical and petroleum industries has led to a proliferation and diversification of air pollutants. On the other hand, the population explosion has led to a considerable increase in energy needs and a consequent increase in car traffic. In this context, the United Nations Framework Convention on Climate Change (Rio de Janeiro, 1997) and these extensions, including the most recent the Paris Agreement, propose to the signatory states to commit themselves to putting in place "flexibility" to reduce greenhouse gas emissions. Of the most polluting sectors, transport accounts for 26% ([ACEA]). The regulation of pollutant emissions and greenhouse gas emissions associated with the fleet is therefore becoming an environmental necessity. To understand the process of automobile pollution, it is essential to control the flow around it.

The flow around a real motor vehicle is very complex, sometimes detached and often strongly three-dimensional. Ahmed & Baumert, (1979) define three types of geometry: the

"squareback" vehicle, the "fastback" vehicle and the "notchback" vehicle. Previous experimental studies ([1], [2] and [3]), make it possible to identify the flow topology that develops around this geometry. This topology is successively presented on the front and back part of the geometry. On the front part, from tomographies and parietal visualizations, [2] observe a separation at 8% of the length L of the geometry. The fluid located beneath this detached web is driven by a rotational movement. On either side of the longitudinal plane of symmetry, the current lines to the wall are wrapped around two foci and escape from the wall forming two contra-rotating vortices. These swirl structures are advected along the pavilion towards the wake zone. They are, however, less energetic than the longitudinal structures that develop along the side edges of the windshield on a real geometry of a motor vehicle.

On the back of the body, the studies of [1], [2], [4], [5] and [6] focus on the influence of the angle of inclination α of the rear window on the topology of the flow and associated drag. for Reynolds number $Re_L = 4.28 * 10^6$, the existence of critical values $\alpha_m = 12.5^\circ$ and $\alpha_M = 30^\circ$. For an angle α less than $\alpha_m = 12^\circ$, the flow remains stuck on the rear window and takes off on the periphery of the base: The flow is said right base; For α between 12° and 30° , the flow takes off on the top of the rear window and partially stuck on the bottom of the rear window: The flow is of the hatch type; Finally, for α greater than 30° , the flow takes off over the entire rear window and the topology suddenly changes to a flow-type right cap. The evolution of the drag as a function of the inclination α also reveals two singular inclinations: the drag curve has a minimum for an inclination of 12° and then a growth phase up to 30° where it decreases abruptly. This variation in the drag is associated with a change in the topology of the flow. Modification that can have various origins.

One approach is to control the phenomenon of delamination of the boundary layer around a profile this is the case of the studies of [7], [8], [9], [10], [11] and [12]. This improves the performance and fuel efficiency of the vehicle. Two types of methods are studied: passive control and active control of the flow. Passive flow control does not require additional energy input. For example, the addition of

longitudinal [7] and transversal separator elements [8], optimization of the engine compartment [13] or of suction wheels, [14], [15], are so many free solutions that do not deteriorate the habitability of the vehicle. The solutions identified are still used but remain highly constrained by market requirements in terms of comfort, livability and safety. The best aerodynamic drag coefficients thus remain close to 0.30 for more than 20 years [16]. To improve this result, new solutions based on breaking geometries and a better knowledge of the aerodynamic drag formation and development processes must be sought.

The active control type solutions require, for their part, a supply of energy external to the flow and rely mainly on the use of fluidic sources of blow or suction type through slits [9], [10] and [17]. The objective is to avoid or delay the separation of the boundary layer from a certain angle of incidence. It is a question of placing actuators on the wings; that is to say, air injectors on the extrados, which force the boundary layer to follow the profile without separating. The simulations and experiments carried out by several teams of researchers [18], [19], [20], tend to prove that their positions as well as other parameters have a significant influence on their effectiveness.

This bibliographic analysis shows that many parameters remain to be exploited. We are interested here, in the influence of the coupling control of the underflow flow and blowing on the flow around the body of Ahmed of the flow velocity and the angle of inclination on the height of the layer limit. Especially when controlling the upstream flow and underbody. To carry out this study, we will present the mathematical model as well as the modeling equations that we used during our simulation.

II. MATERIAL AND METHODS

A. Physical situation

The physical situation corresponds to a three-dimensional, turbulent incompressible natural flow in a wind tunnel where we have imposed velocity values on the turbulent flow. For an individual sequential resolution of the equations we have chosen a decoupled solver in stationary regime. The closing model of the system of equations is turbulent viscosity with two equations (the variants of the model k-ε). The wall function for treating turbulence near walls is a standard function of walls. Finally, it is necessary to set the initial conditions which are the basic state of the model at the moment when the simulation begins. Here, the thermo-physical properties of the flowing fluid and those of the wall in contact with the fluid are evaluated at the initial time.

The numerical resolution of the equations follows the scheme defined by [21]. The integration of the transport equations is done by the finite volume method. This method makes it possible to take into account the presence of obstacles in the flow of the fluids and guarantees the preservation of mass and momentum in the whole field of computation.

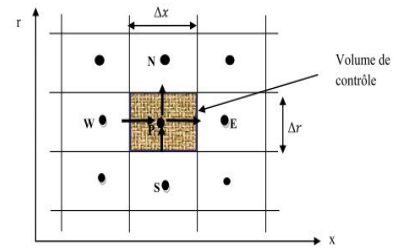


Figure 1. Volumes finis bidimensionnels [22]

The average global transport equation

$$\frac{\partial}{\partial x_j} (\rho \langle u \rangle \psi) = \frac{\partial}{\partial x_j} (\Gamma_\psi \frac{\partial \psi}{\partial x_j}) + s_\psi \quad (1)$$

Will be written in the integral form following Ostrogradski's theorem. We obtain:

$$\int_A n(\rho \psi \langle u \rangle) dA = \int_A n(\Gamma_\psi \text{grad} \psi) dA + \int_V S dv = \quad (2)$$

This equation will be integrated on the control volume during Spatial Discretization. Assuming that the generalized variable ψ varies linearly between the main nodes in both directions, that the convective and diffusive terms are uniform across the corresponding faces and a uniform source term on the control volume; we integrate separately the terms of the transport equation (total flow and the source term). All these transport equations, after having been discretized, will be put into the following generalized linearized form:

$$a_p \psi_p = \sum_{nb} a_{nb} \psi_{nb} + b \quad (3)$$

The discretization scheme of the power law is used because it is less expensive in computing time [23]. The numerical resolution of these equations is not easy and direct especially if the variable is one of the speed components, because the coefficients a_i ($i = E, N, W, S$) appearing in the discretization equation depend of these variables and the source terms of the momentum equations, involve the pressure gradients or we have no equation for this variable so far. Yet, numerical resolution consists of a sequential resolution of the conservation equations of momentum and continuity. This pressure-velocity coupling, which makes the incompressible flows unique, makes the resolution difficult. This is why we choose the SIMPLE algorithm to be able to use pressure in the continuity equation.

B. Governing equations

The Reynolds Averaged Navier-Stokes (RANS) equations solved by fluent are presented there. The RANS approach of permitting a solution for the mean flow variables greatly reduces the computational effort. If the mean flow is steady, the governing equations will not contain time derivatives and a steady-state solution can be obtained economical.

$$\frac{\partial \rho}{\partial t} + \frac{\partial(\rho u_i)}{\partial x_i} = 0 \quad (4)$$

$$\frac{\partial(\rho u_i)}{\partial t} + \frac{\partial(\rho u_i u_j)}{\partial x_j} = \frac{\partial p}{\partial x_i} + A + B \quad (5)$$

Here,

$$A = \frac{\partial(\mu(\frac{\partial u_i}{\partial x_j} + \frac{\partial u_j}{\partial x_i} - \frac{\partial \delta_{ij} \partial u_i}{3 \partial x_i}))}{\partial x_j} \quad (6)$$

And

$$B = \frac{\partial(-\rho u_i u_j)}{\partial x_j} \quad (7)$$

This approach is generally adopted for all practical engineering calculations, and is used with turbulence models. Realizable k- ϵ Turbulence Model:

$$\frac{\partial(\rho \epsilon)}{\partial t} + \frac{\partial(\rho k u_j)}{\partial x_j} = \frac{\partial(\mu + (\frac{u^2}{\sigma_k}))}{\partial x_j} + G_k + G_b - \rho \epsilon - Y_M + S_k \quad (8)$$

$$\frac{\partial(\rho \epsilon)}{\partial t} + \frac{\partial(\rho \epsilon u_j)}{\partial x_j} = \frac{\partial(\mu + (\frac{u^2}{\sigma_\epsilon}))}{\partial x_j} + \rho C_{1\epsilon} S_\epsilon - \rho C_{2\epsilon} \frac{\epsilon^2}{k + \sqrt{\nu \epsilon}} + C_{1\epsilon} \frac{\epsilon}{k} - C_{3\epsilon} G_b + S_\epsilon \quad (9)$$

Here

$$C_1 = \max(0.43 \frac{n}{n+5}) n = S \frac{k}{\epsilon} \quad (10)$$

$$S = \sqrt{2S_{ij}} \quad (11)$$

Here, G_k and G_b are generation of turbulent k- ϵ . due to mean velocity gradients and buoyancy respectively. Y_M is represents the contribution of the fluctuating dilatation in compressible turbulence to the overall dissipation rate. S_k and S_ϵ are user-defined source terms for ϵ and k respectively. Where, $C_{1\mu}$, $C_{1\epsilon}$, and $C_{2\epsilon}$, are empirical constants; σ_ϵ and σ_k are respectively the turbulent Prandtl numbers relative to ϵ and k. The values of these constants proposed by [24], are represented on table 1 bellow.

TABLE I. EMPIRICAL CONSTANCES

C_μ	$C_{1\epsilon}$	$C_{2\epsilon}$	σ_ϵ	σ_k
0.09	1.44	1.2	1.0	1.3

III. RESULT AND DISCUSSION

A. physical modelisation and mesh domaine

The geometry used for numerical simulation in the air is a so-called "Ahmed" body (scale 1/50) [9]. The lower part is underbody and is positioned at a height $h = 0.05$ m from the floor of the digital wind tunnel. This underbody height receives an imposed speed, and is used as a flow control zone. The

velocity V_1 imposed in the basement is lower than the reference velocity V_0 for modeling the velocity deficit in the basement associated with lateral leaks [25]. Four scenarios are envisaged:

TABLE II. CASE STUDY

Case	Case 1	Case 2	Case 3	Case 4
$\eta =$	1	0.6	0.2	0.1

The associated Reynolds number is $Re = 6 * 10^6$. The angle of the rear window α is 25° . The dimensions of the wind tunnel are defined as prescribed by [26]. The pressure on the exit surface is uniform (P_0). The input conditions, applied to the faces on the left of the simulation domain (input), impose a uniform velocity over Ahmed's body and underbody. The flow is advected from left to right and the fluid is initialized at the velocity V_0 at the top of Ahmed's body and V_1 at the base. Finally, a frictionless wall condition is imposed on the floor of the blower and on the geometry.

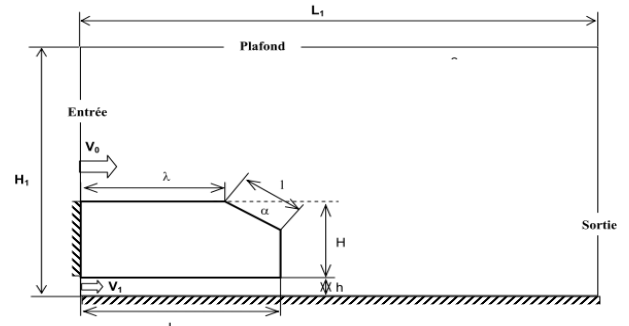


Figure 2. physical modele [9]

The result of the discretization of differential transport equations is a set of algebraic equations. We have therefore divided the computation domain into N meshes according to x, M meshes following y and P meshes following z. We will therefore have a system of $M * N * P$ of nonlinear algebraic equations for each variable considered. An insufficient number of meshes will for example diverge the computation or will be responsible for a numerical diffusion too important whereas a mesh too fine will weigh down the computation or can cause too great variations in the sizes of mesh through the rest of the field. We must therefore find a compromise between the two situations. The choice of the mesh takes into account the influence of this one on the flow velocity. So, as before, we tested different meshes before taking the one that has the least influence on the results. The mesh chosen is the finest. That is, 1.323.337 figures.

The grid distribution is a set of quadrilateral cells (uniformly structured mesh). The mesh is very uniformly fine near of the wall and around the Ahmed Body, where the velocity gradient is large. The grid distribution impacts the computation time and the number of iterations required for the solution converge.

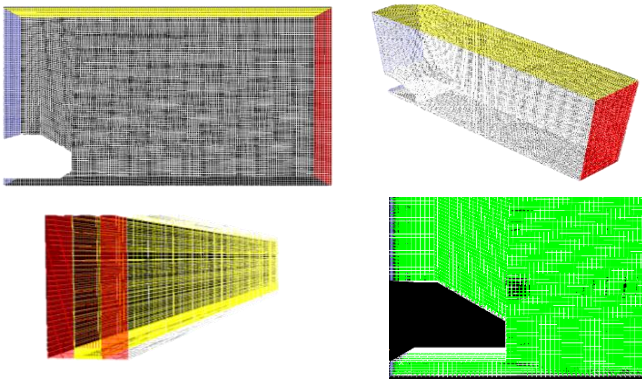


Figure 3. Grid configuration

B. Flow study on the median plane

In general, depending on the flow rate η , two types of flow are observed; for cases 1 and 2, we find the absence of the delamination bulb that characterizes the upstream flow on previous studies. The same results are obtained by [27] which indicate that the introduction of tangential blowing eliminates the detachment that appears when the profile is in incidence. However, for cases 3 and 4, this detachment bulb reappears, and is perfectly present over the entire width of the base (on the Z plane) and seems to have the same profile and the same volume over the entire surface of appearance. Which suggests that this bulb is a function of the blowing speed.

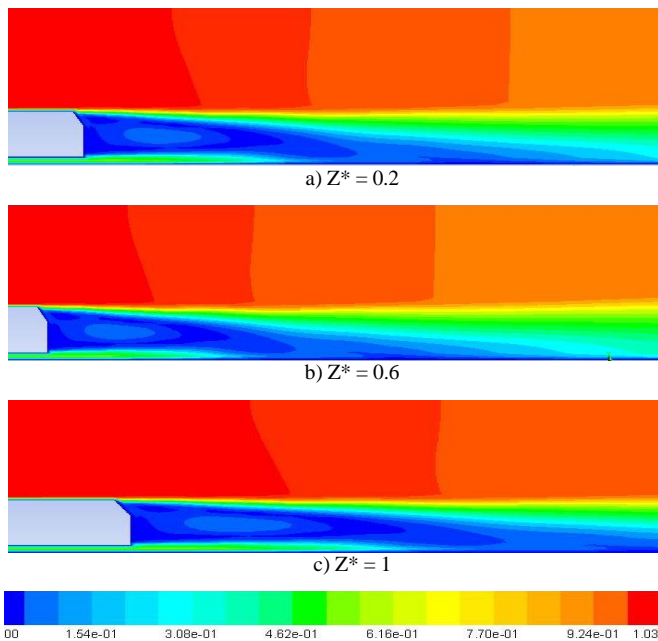


Figure 4. Velocity fields in the median plane for case 1

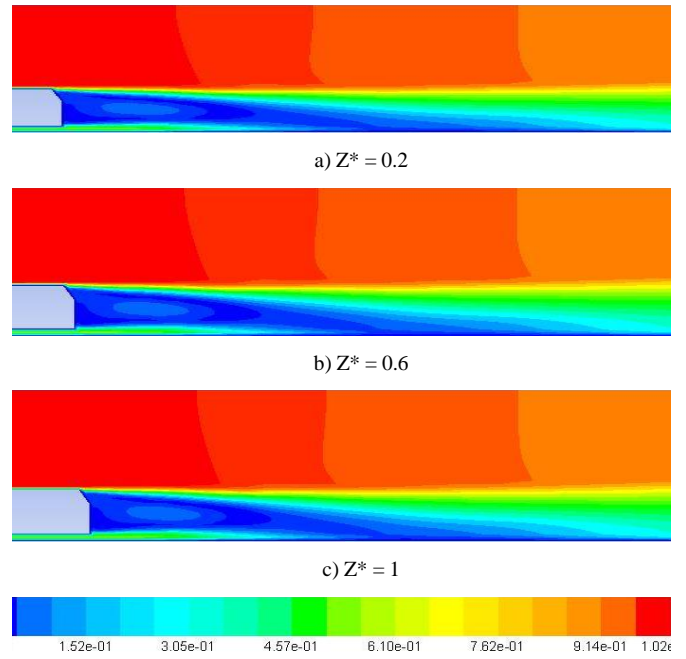


Figure 5. Velocity fields in the median plane for case 2

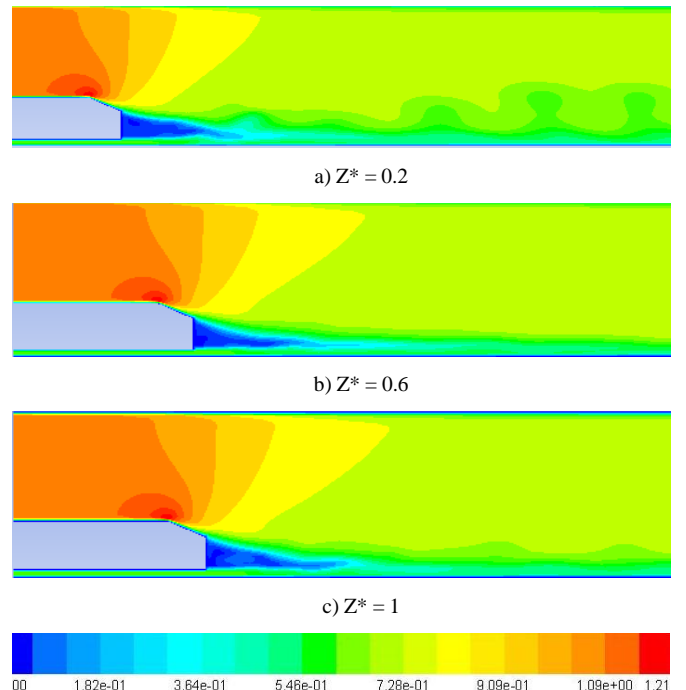


Figure 6. Velocity fields in the median plane for case 3

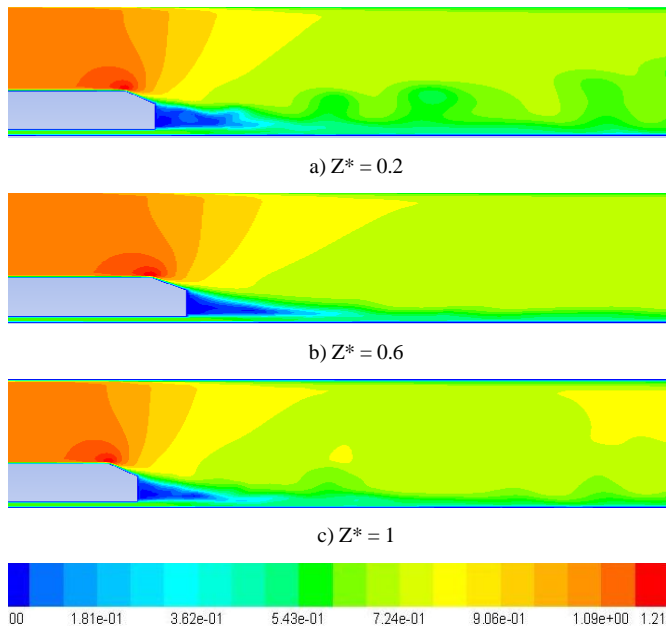


Figure 7. Velocity fields in the median plane for case 4

The symmetry of the flow on the median line makes it possible to observe a transition line which is established between the wake zone where the flow is swirling and the free flow zone. The size of the wake zone seems wider and smaller, unlike the cases without blowing. For cases 3 and 4, it infiltrates slightly in the flow until the end of flag. The recirculation zone is completely closed on the right base.

C. Flow study on the transversal plane

The transversal plane allows us to actually see that the flow at the top of the telescope is perfectly uniform. It allows to observe and characterize the transition zone between the turbulent boundary layer and its under layer. It is progressive until the end of the flag for case 1 as for case 2. The upper vortex begins to take shape at $x^* = 0$, the recirculation zone closes completely at $x^* = 3$ for case 1 and $x^* = 5$ for case 2. We notice the appearance of the sub-boundary layer of [28]. It appears at $x^* = 0.1$ and tends to close the flow at $y^* = 0.17$. The vortex remains close on the height of the right base.

For cases 3 and 4, we can characterize the delamination bulb, which extends between $x^* = -0.9$ and $x^* = -0.4$, for a total length of $L = 0.5$ mm. This large size of bulb is certainly due to the small size of the orifices of the jet which allows according to [9] the amount of movement injected, to remain in the boundary layer thus widening the bulb. The recirculation zone closes completely at $x^* = 1.8$, unlike the other cases. The vortex remains close on the height of the right base. We clearly see the two revolving Centro vortex developing on the middle lines (wider in upper vortex).

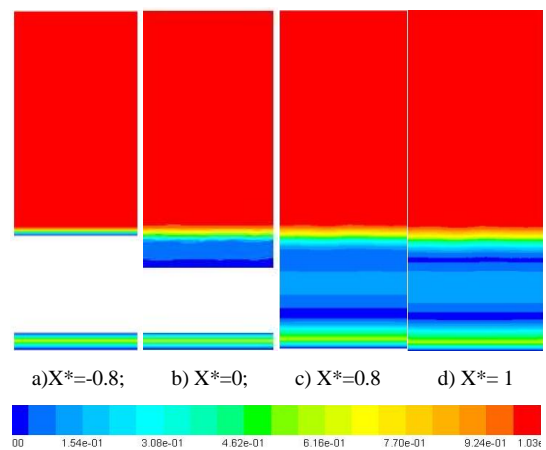


Figure 8. Velocity fields in the cross plane for case 1

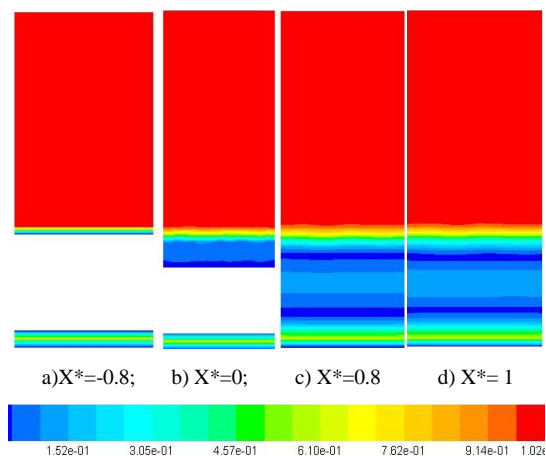


Figure 9. Velocity fields in the cross plane for case 2

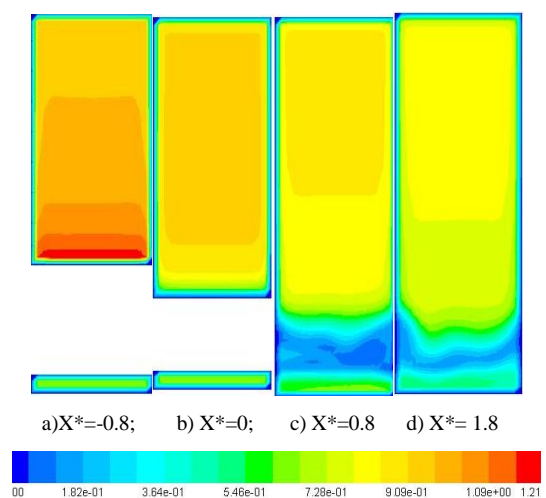


Figure 10. Velocity fields in the cross plane for case 3

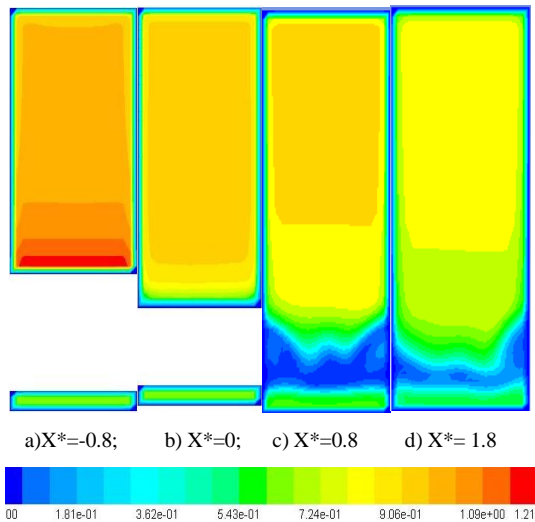


Figure 11. Velocity fields in the cross plane for case 4

D. Flow study on the longitudinal plane

The longitudinal plane allows us to notice that the transition line between the two flow zones is at $y^* = 1.21$. The maximum velocity of the flow is $U^+ = 1.03$. The recirculation zone, for its part, is enclosed between $y^* = 0.2$ and $y^* = 1$ is between the right pellet and the rear window for cases 1 and 2. For cases 3 and 4, it is enclosed between $y^* = 0.2$ and $y^* = 0.6$, and between $y^* = 0.2$ and $y^* = 0.8$. There is only one vortex, the upper vortex disappearing. Thus reducing the cross-sectional area of the wake during blowing as demonstrated in the literature.

For cases 3 and 4, the detachment bulb takes shape as $y^* = 1.2$ and disappears at $y^* = 1.6$ for $n = 0.2$ and for $n = 0.1$, it goes from $y^* = 1.2$ to $y^* = 1.8$ for an adimensioned speed of $U^+ = 1.21$, corresponding to the maximum velocity of the flow.

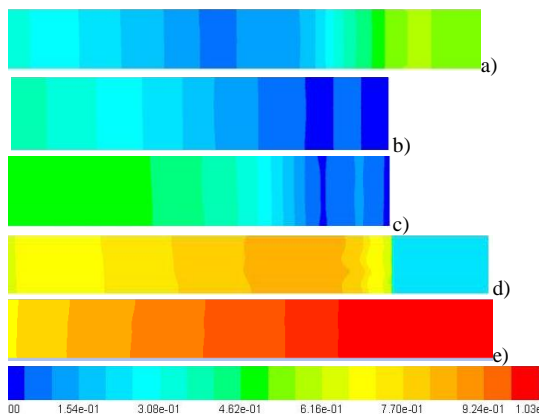


Figure 12. Velocity fields in the longitudinal plane for case 1 in different position a) $y^*=0.1$, b) $y^*=0.4$, c) $y^*=0.8$, d) $y^*=1.2$, e) $y^*=1.3$

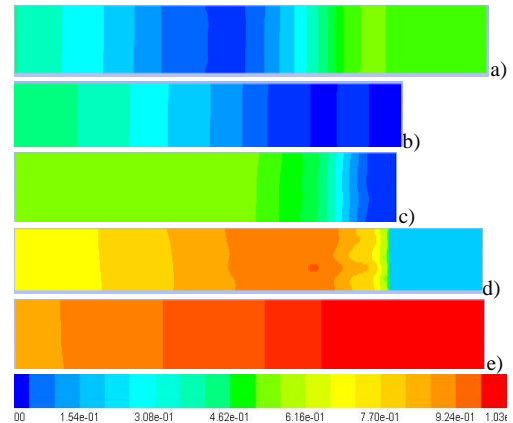


Figure 13. Velocity fields in the longitudinal plane for case 2 in different position a) $y^*=0.1$, b) $y^*=0.4$, c) $y^*=0.8$, d) $y^*=1.2$, e) $y^*=1.3$

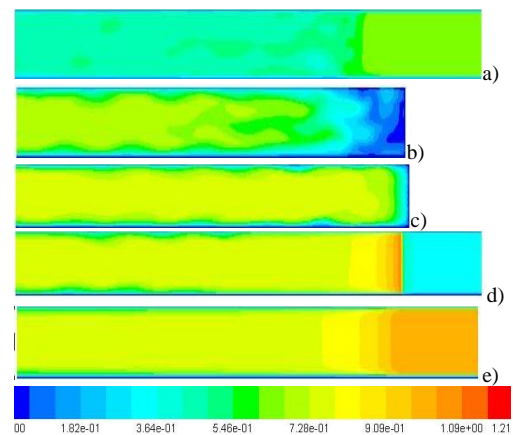


Figure 14. Velocity fields in the longitudinal plane for case 3 in different position a) $y^*=0.1$, b) $y^*=0.4$, c) $y^*=0.8$, d) $y^*=1.2$, e) $y^*=1.3$

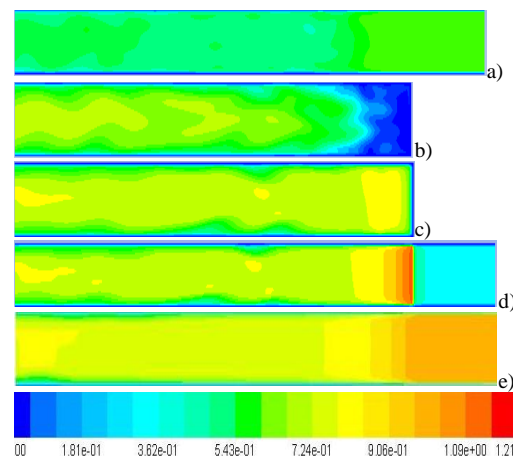


Figure 15. Velocity fields in the longitudinal plane for case 4 in different position a) $y^*=0.1$, b) $y^*=0.4$, c) $y^*=0.8$, d) $y^*=1.2$, e) $y^*=1.3$

In practice, the main purpose of control is to limit total pressure losses by eliminating, or more likely reducing, the development of energy-intensive structures. Thus, having eliminated and repel the separation on the top of the rear window can limit the associated total pressure losses and reduce the cross section S of the wake. Similarly, longitudinal eddies being very energetic, the control made it possible to limit their development.

IV. CONCLUSION

We have been able to demonstrate that the flow in underfloor control with blowing is divided into two types of flow depending on the flow: a flow that we will say of type 2D for a $\eta < 0.5$ and a flow of type 3D for a $\eta > 0.5$. This characterization represents an innovation in research in the field. For a flow rate $\eta > 0.5$, where flow type 3D, the detachment bulb is non-existent in contrast to a so-called flow type 2D. This is certainly due to the fact that the difference between the blowing speed and that of the upstream flow is very small. The transverse plane makes it possible to characterize the transition zone, the upper vortex and the recirculation zone.

REFERENCES

- [1] Ahmed S., Ramm R. & Falting G. (1984). Some salient features of the time averaged ground vehicle wake. SAE technical paper. series 840300, Detroit.
- [2] Spohn A. & Gilliéron P. (2002, April). Flow Separations Generated by a Simplified Geometry of an Automotive Vehicle. Congrès IUTAM Symposium on Unsteady Separated Flows. Toulouse, France.
- [3] Lienhart H., Stoots C. & Becker S., (2002, mois). Flow and turbulence structures in the wake of a simplified Car Model (Ahmed Model). Roc. DGLR Fach. Symp. Der AG STAB. Stuttgart University.
- [4] Gilliéron P. (2000, March). Analyse, modélisation et typologie des écoulements de culot dans l'automobile, AAAF - 36eme colloque d'aérodynamique appliquée.
- [5] Lienhart H. & Becker S. (2002, mois). LDA Measurements of the Flow and Turbulence Structures in the Wake of a Simplified Car Model. 11th International Symposium on Application of Laser Techniques to Fluid Mechanics. Lisbon - Portugal.
- [6] Krajnovic & Davidson "Contribution Large-Eddy Simulation of the Flow Around a Simplified Car Model", SAE International Congress & Exposition N°2004-01-0227, Detroit, Michigan, 2004.
- [7] Gilliéron P. (2001). Analyse de la contribution des plaques séparatrices à la réduction de la traînée aérodynamique. Note interne RENAULT n°0455/64260/2001. France
- [8] Levallois E. & Gilliéron P. (2005, June). Réduction de traînée en aérodynamique automobile par contrôle passif des écoulements – analyse par PIV. Colloque de visualisation et de traitement d'images en mécanique des fluides. - EC Lyon.
- [9] Rouméas M. (2006). Contribution à l'analyse et au contrôle des sillages de corps épais par aspiration ou soufflage continu. Thèse de doctorat n 2348, université de Toulouse, France.
- [10] Leclerc C. (2008). Réduction de la traînée d'un véhicule automobile simplifié à l'aide du contrôle actif par jet synthétique. Thèse de doctorat. – Toulouse, France.
- [11] Aider J., Lasserre J., Beaudoin J., Herbert V. & Wesfreid J. (2009, août). Contrôle d'écoulement en Aérodynamique automobile. 19ème Congrès Français de Mécanique. P 1-6. Marseille, France.
- [12] Kourta & Gilliéron, (2009)
- [13] Ivanic T. & Gilliéron P. (2005, April). Reduction of the aerodynamic drag due to cooling systems: an analytical and experimental approach, SAE. Detroit, Michigan.
- [14] Thivolle-Cazat E. & Gilliéron P. (2005, September). Modèle analytique d'hélice ventilateur pour la conception de roues aspirantes. 17ème congrès Français de Mécanique. Troyes.
- [15] Renault (2007, October). A l'occasion du Challenge Bibendum Michelin, Renault présente Logan "Renault ECO2" concept, véhicule écologique et économique, Direction de la Communication, Communiqué de Press.
- [16] Bruneau C., Gilliéron P. & Mortazavi I. (2007). Passive control around the square back Ahmed body using porous devices. Journal of Fluids Engineering.
- [17] Gosse étude expérimentale de la dispersion d'un scalaire passif dans le proche sillage d'un corps d'Ahmed, thèse de doctorat de la faculté des sciences de l'université de Rouen, 2005
- [18] Smith B. & Glezer A. (1994). "Vectoring of a high aspect ratio air jet using zero-net-mass-flux control jet". Bulletin of American Physical Society. No. 39:1894..
- [19] Greenblatt D. & Wygnanski I. (2000). "The control of flow separation by periodic excitation". Progress in aerospace sciences. Vol. 36, pp. 487-545.
- [20] Smith B. & Glezer A. (2002). Jet vectoring using synthetic jets. Journal of Fluid Mechanics. Vol. 458, pp. 1-24..
- [21] Versteeg H. & Malalasekera W. (1995). An introduction to Computational Fluid Dynamics, the finite volume method. England : Addison Wesley Longman Limited, 1995.
- [22] Patankar Numerical heat transfer and fluid flow./ Mc Graw Hill, 1980.
- [23] Patankar & Baliga A new finite element formulation for convection-diffusion problem, Numerical Heat Transfer, Part B, Vol. 3, 1980.
- [24] Jones & Lauder, (1961)
- [25] Chometon & Gilliéron Modélisation des écoulements tridimensionnels décollés autour des véhicules automobiles à l'aide d'un modèle à zéro-dimension, Journée d'étude SIA « Aérodynamique – Aéroacoustique - Aérothermique automobile et ferroviaire », - Courbevoie-Paris 5 et 6 novembre 1996.
- [26] Chen S. & Doolen G. Lattice Boltzmann Method for fluid flows, Ann. Rev. Fluid Mech., Vol. 30, pp. 329-354, 1998.
- [27] Bourgois S., Alvi F., Tensi J. & Bonnet J. (2004, Octobre). Control of flow separation using microjets, Proceedings of the First European Forum on Flow Control. Poitiers, France.
- [28] Tcheukam-Toko D., Kongue L., Koueni-Toko C. A., Mouangue R. & Bêlorgey M. Numerical Simulation and Experimental Validation of Boundary Layer Generated by a Turbulent Flow on a hydraulically Smooth Bed, Res. J. of Applied Sci., Vol. 7(2), pp.108-112, 2012.